



Interactions of Crucible Materials With an $\text{FeO}_x\text{-SiO}_2\text{-Al}_2\text{O}_3$ Melt and Their Influence on Viscosity Measurements

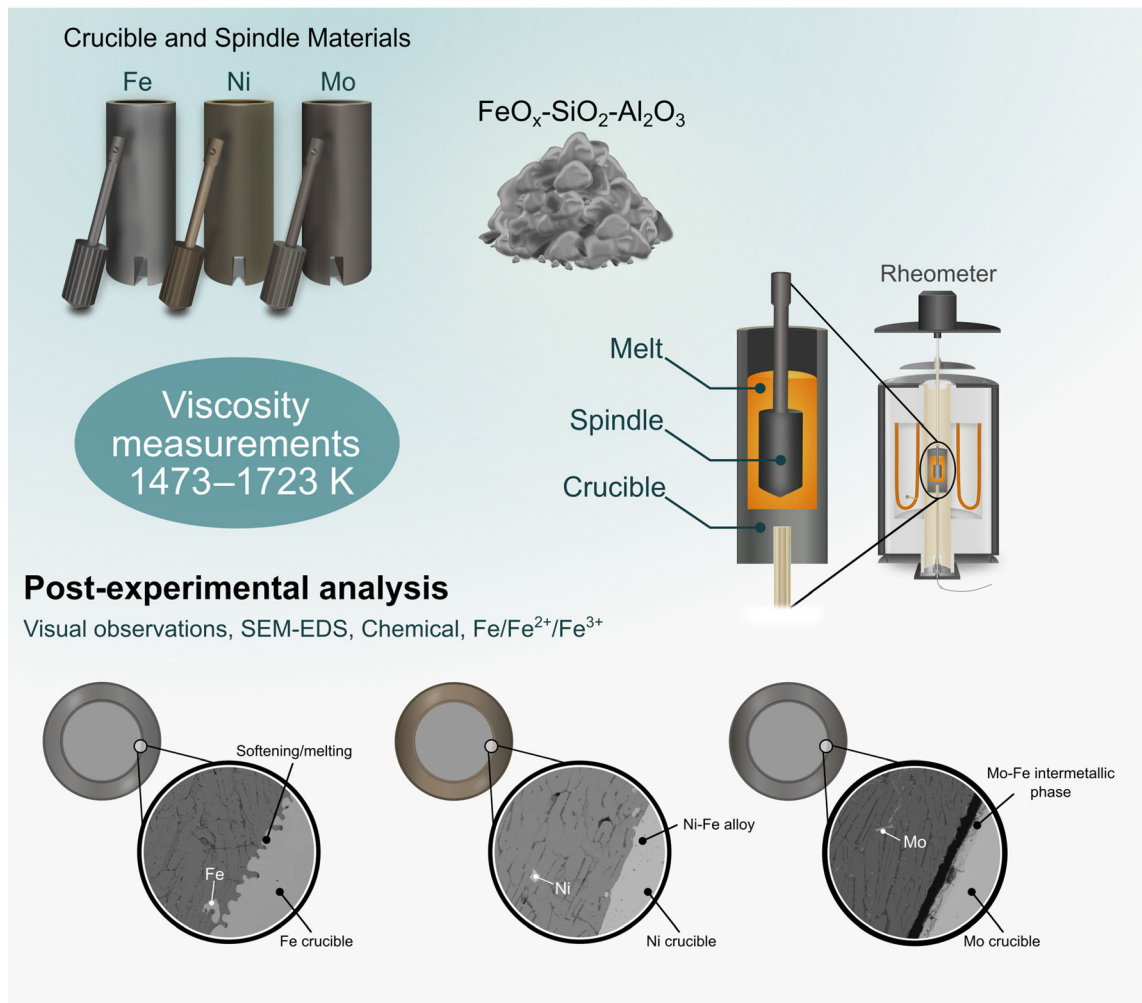
JENNY ISAKSSON, ANTON ANDERSSON, ANDREAS LENNARTSSON,
and CAISA SAMUELSSON

Viscosity is a critical parameter during metal extraction, influencing the settling of valuable droplets, slag handling, and mass transfer. The viscosity of oxide melts can be measured with high-temperature rheometers. During such measurements, interactions between the crucible and the oxide system can change the chemical composition, melt structure, and thus the viscosity. For increased reliability of viscosity measurements, the influence of crucible and spindle materials on viscosity must be studied. In this study, the viscosity of a synthetic $\text{FeO}_x\text{-SiO}_2\text{-Al}_2\text{O}_3$ melt was measured using the rotating spindle technique and three different crucible and spindle materials (Mo, Fe, and Ni) to determine the interactions with the melt and the influence on viscosity. The interaction was evaluated by comparing the post-experimental chemical analyses, the $\text{Fe}/\text{Fe}^{2+}/\text{Fe}^{3+}$ content, visual observations, and using scanning electron microscopy–energy dispersive spectroscopy (SEM–EDS). The results showed that all the crucibles partially dissolved into the melt, affecting the melt structure, composition, and, thus, the viscosities. The viscosity data obtained using the Mo setup interacted the least with the melt, was the most stable, and with the best reproducibility.

JENNY ISAKSSON, ANTON ANDERSSON, ANDREAS LENNARTSSON, and CAISA SAMUELSSON are with the Division of Minerals and Metallurgical Engineering, Luleå University of Technology, 971 87 Luleå, Sweden. Contact e-mail: jenny.isaksson@ltu.se

Manuscript submitted March 1, 2023; accepted September 21, 2023.

Article published online October 6, 2023.



<https://doi.org/10.1007/s11663-023-02930-1>
© The Author(s) 2023

I. INTRODUCTION

VISCOSITY is one of the physicochemical properties influencing pyrometallurgical processes during metal extraction. The viscosity affects the settling rate^[1] of valuable metals in melts, slag tapping, gas permeability, mass and heat transfer,^[2] kinetics of slag-metal reactions,^[3] furnace refractory life and freeze linings of a water-cooled reactor.^[4] The viscosity thus influences the efficiency of pyrometallurgical operations. Pyrometallurgical processes require accurate viscosity data to optimize the processes and slag composition. The viscosity of an oxide system can be measured with a high-temperature rheometer, *e.g.*, where a spindle rotates in a melt contained in a crucible. Studies have been conducted on simple and more complex oxide systems, but differences are still relevant in the high-temperature viscosity data.^[5,6]

Mills *et al.*^[7] performed a study where reference materials were sent to individual laboratories for viscosity measurements to evaluate the accuracy of the measurements between the laboratories. The overall spread of the measurements from the different laboratories was ± 10 pct around the mean. Few laboratories perform complete chemical analyses of their post-experimental samples, and changes in composition could give rise to a further ± 10 pct variation in the accuracy of the viscosity data. The study concluded that viscosity-temperature-composition data are subjected to uncertainties of ± 20 pct.^[7] The differences could be due to the rheological instrument used, the thermocouple position during the measurements, the atmosphere in the furnace, crucible and spindle geometries, methodology, partial pressure of oxygen ($p\text{O}_2$), and change in melt composition during measurements.

Viscosity measurements in molten oxide systems are often performed at temperatures above 1373 K and for a long time (>10 hours). One parameter to consider is the interactions between the melt and the crucible and spindle material (*c/s* material) during measurements, and select a *c/s* material that affects viscosity measurements the least. To determine the interaction and the effect on viscosity, it is necessary to use the same rheometer and methodology to isolate the *c/s* material as a single factor.

A. Crucible Options for Viscosity Measurements of an FeO–SiO₂-Based System

A wide range of *c/s* materials has been used for viscosity measurements, including ceramic and metallic materials such as Al₂O₃, MgO, C, Fe, Ni, Mo, Pt, and Pt/Rh. The commonly used slag system is based on FeO and SiO₂ (fayalite-based) for pyrometallurgical extraction of the base metals copper and nickel. The main difference between the FeO–SiO₂–Al₂O₃ system and, *e.g.*, copper slag from a smelting furnace is the presence of the stable oxides CaO and MgO and minor elements such as Cu, Sb, As, Sn, and Pb.^[8–12] If a crucible and spindle system is identified with limited interaction with the FeO–SiO₂–Al₂O₃ system, this can be applied to a more complex system that reflects the complete component system of an FeO–SiO₂-based slag used in pyrometallurgical extraction of base metals.

Challenges with the FeO–SiO₂ system and the selection of *c/s* material during viscosity measurements were identified as (i) to control the pO₂ to avoid oxidation/reduction of FeO, (ii) minimum changes of the crucible and spindle geometries due to the interaction with the melt, and (iii) choose a *c/s* material that allows controlled variations of the melt composition and minimum dissolution into the molten oxide system.

Concerning the first point, controlling the pO₂ in the system, the pO₂ will determine the oxidation state of iron, which will affect the melt structure and, thus, the viscosity. FeO is an impurity present in most industrial slags related to base metal production and usually exists in the two oxidation states Fe²⁺ and Fe³⁺. FeO is reduced in contact with graphite, which excludes this *c/s* material as an option. Reddy and Zhang^[13] performed viscosity measurements of industrial lead slags with various compositions in the temperature range from 1050 °C to 1300 °C using graphite crucibles and spindles. Fuming occurred in the slag at temperatures above 1100 °C due to the reduction of oxides in the melt.^[13] The fuming indicated that the composition changed and mentioned as a source of error.

Besides reducing conditions, pO₂ can also affect the viscosity measurements through melt oxidation. Wang *et al.*^[14] studied the effects of the Fe/SiO₂ ratio and the Fe₂O₃ content on viscosity in a synthetic FeO–Fe₂O₃–SiO₂–CaO–MgO–Al₂O₃ slag. The viscosity increased with increased Fe₂O₃ content when the Fe/SiO₂ ratio was 1.2, and the opposite occurred when the Fe/SiO₂

ratio was 1 and 0.8. The effect on the viscosity was attributed to the amphoteric behavior of Fe₂O₃, which behaved as a network-breaking basic oxide at the low Fe/SiO₂ ratios and as an acidic oxide network forming oxide at higher Fe/SiO₂ ratios. At higher Fe/SiO₂ ratios, tetrahedral [FeO₄]^{5–} forms a more complex network structure with the tetrahedral [SiO₂]^{4–}, which results in increased viscosity.^[14] Viswanathan *et al.*^[3] measured the viscosity in an Fe–O–Si slag using the rotating cylinder technique under an oxidizing CO₂/CO atmosphere at 1623 K and 1673 K. As the oxidation progressed, more Fe³⁺ was formed in the slag. During the initial oxidation, the viscosity remained with a slight decrease at 1623 K. However, the viscosity drastically increased after some time, which was correlated to when the Fe₂O₃ content reached around 7 wt pct and the precipitation of magnetite.^[3] The effect of the oxidation state of Fe on viscosity highlights the importance of controlling pO₂.

The *c/s* material can affect the pO₂ in the melt through the slag–crucible interaction and, thus, the Fe₂O₃ content. One approach to control the pO₂ in the melt is to use an Fe crucible. According to Mysen and Richet,^[15] using a Fe crucible material in high-temperature experiments will provide an oxygen buffer to the system that will approach Fe–FeO conditions.

Regarding the second challenge, minimizing the change in geometries due to interactions with the melt during viscosity measurements refers to the fact that the viscosity data are a function of the measured torque at a specific rotation rate and the geometry constants. When the temperature increases, a thermal expansion of the *c/s* materials will influence the geometries. The linear coefficient of thermal expansion (10^{–6} °C^{–1}) for Mo, Al, Pt, Fe, and Ni are 4.9, 7.4, 9.1, 11.4, and 13.3, respectively.^[16] The difference in the coefficient means that the geometries of the *c/s* material will differ at elevated temperatures where Ni will expand the most.

One obvious disadvantage with Ni and Fe as *c/s* materials is the low melting points of 1728 K and 1811 K (1455 °C and 1538 °C).^[16] Chen *et al.*^[5] performed high-temperature experiments using Fe as *c/s* material, they observed that the spindle and crucible geometries changed at temperatures above 1723 K (1450 °C). The melting points define the upper-temperature limit of the viscosity measurements.

Chen *et al.*^[5] performed viscosity measurements using a Mo spindle and crucible and reported that the geometries remained at the highest experimental temperature of 1773 K (1500 °C). An advantage of using Mo as a *c/s* material is the melting point of 2890 K (2617 °C).^[16] The melting point of Mo allows a wide temperature range during viscosity measurements, which covers operating temperatures in pyrometallurgical base metal processes.

Interactions between the melt and the crucible can change the bulk composition and cause the appearance of solid phases.^[17] The geometries of the *c/s* materials can change due to the formed solids that, *e.g.*, can attach to

the spindle/crucible, affecting the viscosity measurements. The reviewed literature has not reported this phenomenon and its influence on viscosity measurements.

The third challenge is choosing a *c/s* material that allows controlled variations of the melt composition and minimum dissolution of the *c/s* material into the melt. No crucible is inert in contact with an oxide melt at high temperatures. One option for choosing *c/s* materials is to use ceramic materials such as Al_2O_3 and MgO . However, one drawback is the solubility in the FeO-SiO_2 system,^[18] which limits the option to vary the content of these oxides in a controlled way.

The dissolution of Al_2O_3 in molten slags is well-known and reported in the literature.^[19–23] One way to overcome this is to saturate the melt with Al_2O_3 , with the limitation that the content of Al_2O_3 can not be a factor. The Al_2O_3 content in base metal extraction is of interest as it varies with, *e.g.*, the amount of secondary raw materials feed in the process.^[24] Nagraj *et al.*^[4] used an Al_2O_3 spindle and crucible to measure viscosity in zinc fuming slag with main components FeO and SiO_2 and minor oxides Al_2O_3 , CaO , ZnO , PbO , Cu_2O , and Cr_2O_3 . In an equilibrium study before the viscosity measurements (1523 K), the Al_2O_3 content increased by an average of 0.4 wt pct at the slag-crucible interface.^[4] No post-experiment analysis of the slag composition was reported after the actual viscosity measurements.

Because of the strong interaction between ceramics (*e.g.*, Al_2O_3 and MgO) and the FeO-SiO_2 system, more inert materials such as Pt and Pt/Rh are commonly used as *c/s* materials. However, Pt forms a continuous solid solution with Fe.^[15] The alloying between these two metals will change the composition of the melt, and oxygen will be lost. Park *et al.*^[25] measured the viscosity in an $\text{FeO}_x\text{-SiO}_2\text{-Al}_2\text{O}_3$ system using a Pt-10 mass pct Rh crucible and spindle to minimize contamination of the molten material.^[25] No spindle or crucible dissolution was mentioned, nor if an Fe-Pt alloy was formed in the crucible. FeO_x represents the sum of all oxidation states of Fe. Viswanathan *et al.*^[3] used Pt as *c/s* material for viscosity measurements in an FeO-SiO_2 system, the crucible developed cracks during the measurements resulting in damage to the experimental assembly. Pt is thus not a material that can be used for the spindle and crucible during viscosity measurements in the relevant oxide system. The crucibles that remain to be studied are Mo, Ni, and Fe. These metals as *c/s* material will thus be reviewed in more detail in the upcoming literature referring to the dissolution during viscosity measurements.

Wang *et al.*^[14] and Jin *et al.*^[26] measured the viscosity in a synthetic $\text{FeO-Fe}_2\text{O}_3\text{-SiO}_2\text{-CaO-MgO-Al}_2\text{O}_3$ slag using the rotational technique and Mo crucible and spindles. Both studies stated that there was no significant change in composition after the viscosity measurements and that the MoO_3 content was almost negligible. This implies that Mo is a viable choice as a *c/s* material. However, neither the interaction between the crucible and the melt nor its viscosity effect was evaluated.

Chen *et al.*^[5] compiled viscosity data of the FeO-SiO_2 system at 1623 K (1350 °C) from different researchers, and a significant discrepancy was observed. It was not possible to identify one specific reason for the differences in data from the given information. They studied the viscosity of an FeO-SiO_2 system in equilibrium with metallic Fe using a Mo spindle and crucible, less than 0.5 wt pct MoO_3 was reported dissolved into the slag.^[5] Kaiura *et al.*^[27] measured the viscosity in FeO-SiO_2 slags with various amounts of CaO using a rotating spindle technique with Mo as the *c/s* material. X-ray diffraction (XRD) analysis performed after the measurements revealed no Mo compounds.^[27] It was possible that small amounts of Mo dissolved into the melts during the measurements but were below the detection limit for the XRD. Chen *et al.*^[28] used the rotating cylinder technique when performing viscosity measurements of a synthetic $\text{FeO-SiO}_2\text{-Al}_2\text{O}_3$ system, with Mo as the *c/s* material and in an Ar atmosphere; the melt was in equilibrium with metallic Fe during the viscosity measurements. The authors did not mention any dissolution of the *c/s* material into the melt or the oxidation state of Fe.

Viswanathan *et al.*^[3] measured the viscosity of an $\text{FeO-Fe}_2\text{O}_3\text{-SiO}_2$ system using Fe and Ni crucibles under an argon atmosphere and an oxidizing atmosphere with a CO/CO_2 gas mixture. The viscosity measurements with the Ni and Fe crucibles agreed, indicating that Ni can be used as a *c/s* material. No post-experimental analysis was presented. However, Ni oxidation was likely due to the lowering of NiO activity formed due to dissolution in the slag.^[3]

Various *c/s* materials have been used for viscosity measurements in the reviewed literature, and post-experimental analysis is often performed and mentioned in the publication. However, the interaction between Mo, Ni, and Fe and the melt and the influence on viscosity is rarely investigated and reported.

B. The Objective of This Work

Knowledge of the crucible and spindle interaction with the melt and the influence on high-temperature viscosity must be increased to obtain reliable viscosity data. The uncertainties of viscosity data from different laboratories^[7] make it difficult to determine the contributions of instruments and methodologies and the crucible and spindle interaction with the oxide system. To study the interaction, using the same rheological equipment and method to isolate the *c/s* material as a single factor is necessary.

This study examined the interaction between the *c/s* materials, Mo, Fe, and Ni, and the $\text{FeO}_x\text{-SiO}_2\text{-Al}_2\text{O}_3$ system and the effect on viscosity measurements. The interaction between the *c/s* material and the oxide system was determined by performing viscosity measurements, calculating and comparing the activation energies, and performing post-experimental analyses, including chemical analyses, determination of the oxidation state of Fe,

visual observations of the *c/s* material and SEM–EDS analysis. Three replicates were performed for each type of *c/s* material to obtain information about the reproducibility and stability of the viscosity measurements in the rheological equipment. The study was conducted to choose a *c/s* material for viscosity measurements in a fayalite-based system (FeO–SiO₂) to enhance the reliability of viscosity experiments in expanded systems. This study obtained more insight into the origin of errors during high-temperature viscosity measurements and improved the reliability and reproducibility of viscosity measurements.

II. EXPERIMENTAL

A. Preparation of Reference Material

The reference material used in this study was an FeO–SiO₂–Al₂O₃ oxide system with an Fe/SiO₂ ratio (wt pct/wt pct) of 1.8. The material was synthesized using an Fe powder (99 pct purity), Fe₂O₃ (98 pct purity), and SiO₂ (99.5 pct purity). All chemicals were from Alfa Aesar, Thermo Fisher, Germany. The components were mixed and packed in an Al₂O₃ crucible (99.7 pct purity) and heated to 1523 K (1250 °C) in a Ruhstrat resistance furnace using a N₂ atmosphere (99.996 pct purity, supplied by Linde Gas AB, Sweden) with a flow rate of 10 L/min. The material was held at 1523 K for 1.5 hours to allow the material to become a homogeneous melt and was then cooled with the natural cooling inside the furnace. Al₂O₃ was allowed to dissolve from the crucible during the synthesis yielding the three-component system FeO_x–SiO₂–Al₂O₃. The dissolution during the syntheses determined the Al₂O₃ content in the reference material. The obtained material was separated from the crucible, crushed, and mixed into one bulk material. Representative samples of the reference material were used for all rheological measurements.

B. Viscosity Measurements

The rotating cylinder technique and three *c/s* materials, Mo (tzm molybdenum 364), Fe (armco pure iron), and Ni (nickel 201/2.4068), were used for viscosity measurements to investigate the interaction between the *c/s* materials and the melt and the influence on viscosity. The rheometer system was an Anton Paar Furnace Rheometer System (FRS 1800)^[29] with a dynamic shear rheometer measuring head with an air-bearing (DSR 502) for precise measurements of the torque at different shear rates.

The crucible and spindle dimensions and a schematic of the rheometer are shown in Figure 1. The crucible inner radius, r_c was 15 mm, the spindle radius, r_s was 9.5 mm, the spindle length, L , was 30 mm, and the cone angle was 120 deg. The measuring position of the spindle was 9 mm above the crucible bottom (d , in Figure 1). The crucibles were attached to an Al₂O₃ shaft covered with a graphite sleeve to prevent oxygen from leaking and entering the system. A precision-lift motor

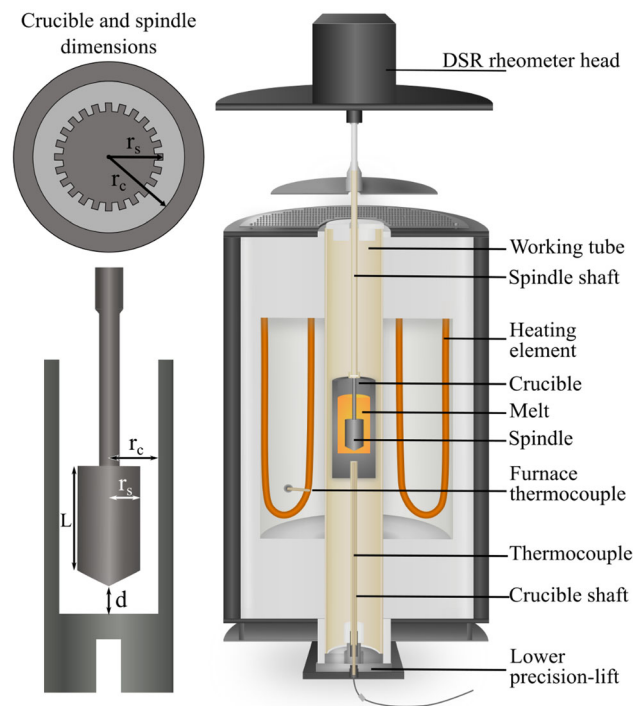


Fig. 1—Crucible and spindle dimensions (upper-left is the top view, and the lower left is the front view). The rheometer is presented to the right.

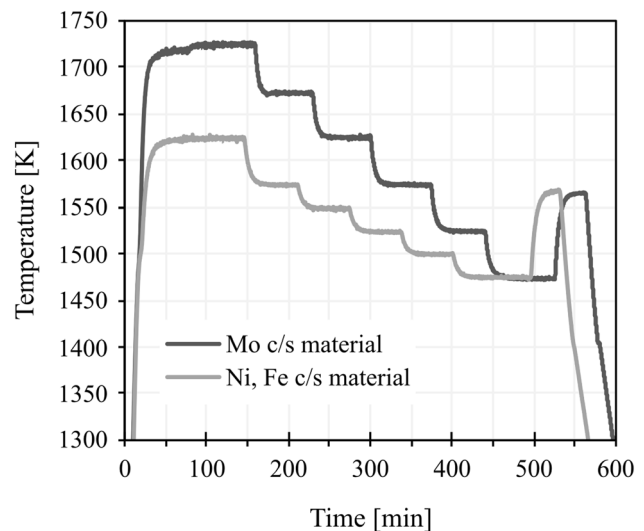


Fig. 2—Temperature profiles of the viscosity measurements using Mo, Ni, or Fe as the *c/s* material.

system controlled the position of the spindle and the crucible. The whole system, including the furnace control, spindle position, and rheometer measurements and shear rates, was preset and controlled by RheoPlus software.

The furnace temperature was controlled with a B-type thermocouple located in the furnace outside the working tube (“Furnace thermocouple” in Figure 1). The temperature, approximately 5 mm from the bottom of the melt, was registered with an additional B-type

thermocouple (Thermocouple in Figure 1). Ar (99.999 pct purity, supplied by Linde Gas AB, Sweden) was introduced into the furnace *via* the crucible shaft using a constant flow rate of 2.5 L/min during the experiment.

The temperature profiles for the viscosity measurements using Mo, Fe, and Ni as *c/s* materials are presented in Figure 2. The furnace temperature was first increased to the highest experimental temperature of 1723 K (1450 °C) using Mo as *c/s* material and 1623 K (1350 °C) using Fe or Ni as *c/s* material. The temperature was kept for 60 minutes while rotating the spindle with a shear rate of 1 s^{-1} to achieve thermal equilibrium (first plateau to the left in Figure 2). The spindle was lowered when the heating started and descended continuously as the material melted until it reached the measuring position. The viscosity was measured at six temperatures during the cooling cycle from 1723 K to 1473 K (1450 to 1200 °C) with 50 K steps when Mo was the *c/s* material, and 1623 K, 1573 K, 1548 K, 1523 K, 1498 K, 1473 K (1350 °C, 1300 °C, 1275 °C, 1250 °C, 1225 °C, and 1200 °C) when using Fe and Ni as *c/s* material. The viscosity was measured with smaller temperature steps using Fe and Ni to obtain six measurements at different temperatures.

Before measurements at a new temperature, the furnace was held for 30 minutes while the spindle rotated with a constant shear rate of 4 s^{-1} . Constant viscosity at a fixed shear rate indicated a homogenized melt. When the measurements were finalized, the temperature was raised, and the spindle was removed from the melt. The furnace was then turned off, and the sample was slowly cooled in the furnace while maintaining the Ar atmosphere. In this rheometer setup, it is not possible to quench samples. Three replicates of each experiment were performed with each *c/s* material, resulting in nine independent runs conducted in randomized order.

The rheometer was calibrated under controlled conditions using reference oils by Anton Paar after being manufactured. The performance of the furnace rheometer system was controlled by measuring the viscosity in Standard glass 1 of the Deutsche Glastechnische Gesellschaft (DGG1) with a viscosity of 93.2 Pa s at 1473 K (1200 °C). This was done to check if the system works well, including temperature, calibration, adjustments, and the motor. The rheometer, equipped with an air-bearing rheometer head, allows quantification of the viscosity in the range from 0.001 to 10^7 Pa s.

C. SEM–EDS

The post-experimental material from one of the replicate viscosity measurements of each crucible/spindle setup was subjected to analysis using SEM–EDS. A disc was cut from one crucible of each setup, giving a cross-section of the crucible and the solidified melt. These samples were mounted in epoxy, polished using a standard metallographic procedure, and carbon-coated before the analysis. The phases and the interaction with the crucibles were determined using a Zeiss Gemini Merlin SEM (Zeiss, Oberkochen, Germany) and analyzed quantitatively using an Oxford

Instruments X-Max EDS (Oxford Instruments, Abingdon, UK) detector. The SEM had an accelerating voltage of 20 keV, an emission current of 1 nA, and a working distance of 8.5 mm. Before the analysis, the beam measurement calibration for the EDS was performed on pure copper. The elemental compositions were reported in wt pct and normalized, meaning that the sum of the elements was 100 wt pct.

D. Chemical Analyses

A disc was cut from each crucible setup for SEM–EDS analysis, and the remaining material was removed and ground using a ring mill. A representative sample of the post-experimental material was taken from one of the replicate viscosity measurements of each *c/s* material setup, and the chemical composition was analyzed using an XRF (Malvern Panalytical, Malvern, UK). The contents of Fe, Fe^{2+} , and Fe^{3+} were determined by titration according to ISO 2597-1:2006 without reduction with tin(II) chloride and ISO 2597-2:2008 without reduction with titanium(III) chloride and the XRF analysis. The XRF analysis determined the total Fe content, and the Fe and Fe^{2+} contents were determined by titration with potassium dichromate. The Fe^{3+} content was calculated by subtracting the Fe and Fe^{2+} contents from the total Fe content. The chemical analyses of the post-experimental material were then compared with each other and the synthesized reference material. The composition of the reference material may change continuously during the viscosity measurements and can be affected by the interaction with the crucible and spindle material, the pO_2 , and slow cooling. All samples were, however, treated in the same way and thus compared with each other.

E. Thermodynamic Calculations

The theoretical pO_2 and liquidus temperature were calculated based on the post-experimental compositions using the different *c/s* materials. It was assumed that the thermodynamic equilibrium was reached for the calculations, but this was not verified. The calculations were performed utilizing the Equilib module of FactSage 8.1^[30] (FS) with the FToxid and FactPS databases. The viscosity of the reference material and the post-experimental composition using the different *c/s* materials was calculated using the Viscosity module in FS and the Melts database. The contents of Mo and S were excluded because they were not included in the Melts database. The Fe_{met} content was recalculated as FeO.

III. RESULTS AND DISCUSSION

In this study, the interaction between the *c/s* materials and a melt and their influence on viscosity were investigated using the same methodology and rheometer and by performing post-experimental analyses, including visual observations, chemical analysis, Fe, Fe^{2+} , and Fe^{3+} determination, and SEM–EDS analysis. Three

replicate experiments were performed for each *c/s* material to determine the reproducibility of the viscosity data.

A. Chemical Analyses

The chemical analysis of the post-experimental materials and a sample of the reference material (Ref.) before the measurements are presented in Table I. The Fe/SiO₂ ratio in the samples varied between 1.76 and 1.83. The content of Mo was 0.43 wt pct in the post-experimental material using Mo as the *c/s* material, and the Ni content was 0.25 wt pct in the post-experimental material using Ni as the *c/s* material. The measurements using the Mo setup started at 1724 K, 100 K above the highest temperature using the Fe and Ni setups. The partial dissolution of the crucibles was assumed to increase over time if equilibrium was not reached, meaning that the content of the *c/s* materials in the melt was lowest at the beginning of the viscosity measurements. It was difficult to determine the partial dissolution of the Fe *c/s* with the post-experimental chemical analysis, as the reference material contained Fe oxides. However, the total Fe content (Fe_{tot}) was higher in the post-experimental material using Fe as *c/s* material than when using Mo and Ni, indicating the dissolution of Fe into the melt.

The Fe_{met}, FeO, and Fe₂O₃ contents in the post-experimental material are presented in Figure 3, together with the contents in the reference material before the viscosity measurements. The figure reveals that the valance state of Fe varied between the samples and was dependent on the *c/s* materials used; the Fe_{met} content was lowest and highest when measurements were made with the Fe crucible and the Ni crucible, respectively. Estimates of pO₂ using the different crucibles were made using the Fe₂O₃ and Fe_{met} contents in the post-experimental materials. Fe_{met} was the highest, and the Fe₂O₃ content was the lowest when using the Fe setup, meaning that Fe²⁺/Fe³⁺ was reduced to metallic Fe. The Fe_{met} content was lowest, and the Fe₂O₃ content was highest when Ni was used as the *c/s* material, meaning that metallic Fe was oxidized to Fe²⁺ or Fe³⁺. Thus, pO₂ was higher in the melt when using the Ni *c/s* material than when Fe and Mo were used. The calculated pO₂ in the post-experimental materials at 1623 K (1350 °C) was 1.6 × 10⁻⁸ atm using Fe, 4.6 × 10⁻⁸ atm using Mo, and 3.3 × 10⁻⁷ atm using Ni; pO₂ increased with increasing temperature for all

compositions. The order of increasing pO₂ was the same at all temperatures and consistent with the content of Fe_{met}, FeO, and Fe₂O₃ using the different *c/s* materials. The pO₂ in the reference material at 1623 K was calculated to be 1.87 × 10⁻⁹ atm, indicating that it increased after interacting with the crucibles during the viscosity measurements.

The liquidus temperature was calculated as 1452 K (1179 °C) for the reference material, 1454 K (1181 °C) when using Fe as the *c/s* material, 1436 K (1173 °C) when using Mo, and 1446 K (1163 °C) when using Ni. The calculated liquidus temperatures implied that the reference material was fully liquid at all temperatures during the viscosity measurements regardless of the *c/s* material. However, one drawback with the equilibrium calculations using FS was that Mo was not included in the database FToxid, which meant that the calculations did not display a possible phase containing Mo in the oxide system.

B. Visual Observations

The post-experimental *c/s* materials were visually observed, and images from one of the replicates for each material are shown in Figures 4(a)–(c). The post-experimental Fe setup is shown in Figure 4(a).

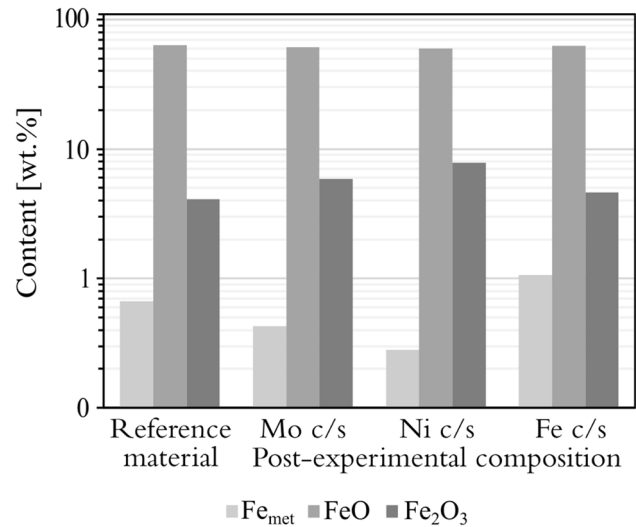


Fig. 3—Fe_{met}, FeO, and Fe₂O₃ contents in the reference material before viscosity measurements and in the post-experimental materials using Mo, Ni, or Fe as *c/s* material.

Table I. Normalized Chemical Analysis of the Reference Material and the Post-experimental Material Using Mo, Fe, and Ni as the *c/s* Material and the Fe/SiO₂ Ratio

<i>c/s</i> Material	Wt Pct/Wt Pct		Wt Pct							
	Fe/SiO ₂	SiO ₂	Al ₂ O ₃	Mo	Ni	S	Fe _{met}	FeO	Fe ₂ O ₃	Fe _{tot}
Ref.	1.83	28.9	2.47	—	—	0.23	0.67	63.6	4.10	53.0
Mo	1.79	29.2	2.40	0.43	—	0.23	0.43	61.4	5.87	52.3
Ni	1.76	29.4	2.58	—	0.25	0.25	0.28	59.4	7.80	51.9
Fe	1.83	28.9	2.56	—	—	0.24	1.07	62.6	4.64	53.0

Fe_{tot} is the total Fe content.

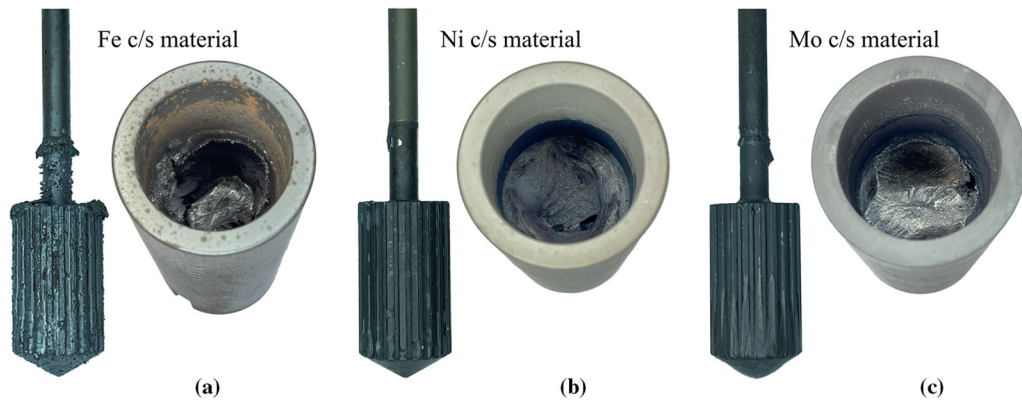


Fig. 4—Post-experimental images of the spindle and crucible: (a) Fe, (b) Ni, and (c) Mo.

The Fe spindles appeared to interact with the molten reference material, and solid particles were observed on the cylindrical bob and shaft. The solid phases on the spindle could increase the measured viscosity as a higher shear force was needed to rotate the spindle when the geometry changed. Therefore, the Fe spindle was replaced with a new one before each experiment. In the crucible, a solid metallic phase was observed at the liquid level during the viscosity measurements, indicating that the *c/s* material and the melt interacted.

The interaction between the reference material and the Fe crucible was indicated when removing the solidified material from the crucible. It was stuck on the crucible wall and had to be scraped off, thus not completely removed. Consequently, the melt interface with the Fe crucible could not be examined as it was scraped off.

The post-experimental Ni *c/s* material is shown in Figure 4(b), and the Mo *c/s* material is shown in Figure 4(c). The Ni and Mo spindle geometries were maintained after each measurement; these spindles were thus used for all replicates. Visual observations showed no interaction between the melt and the crucibles at the liquid level when the material was molten (upper darker level within the crucibles). However, MoO₃ has a high vapor pressure, meaning that Mo could be lost in the form of vapor during the measurements. Traces of a white powder was observed on the outer wall of the crucible, which could be MoO₃. The composition was not confirmed due to the small quantity.

When the disc for SEM-EDS analysis was cut from the Ni crucible, and the solidified melt was removed, bubbles were observed near the interface between the Ni crucible and the oxide phase. The cross-section of the disc is shown in Figure 5(a), and the solidified material after removal from the Ni crucible is shown in Figure 5(b). The bubbles were observed evenly throughout the interface between the Ni crucible and the solidified melt. The traces of bubbles indicates that a reaction has occurred between the melt and the Ni crucible during the viscosity measurements. Clean edges were obtained when the solidified melt was removed from the Mo and Ni crucible. No bubbles were observed in the post-experimental material from the Mo crucible.

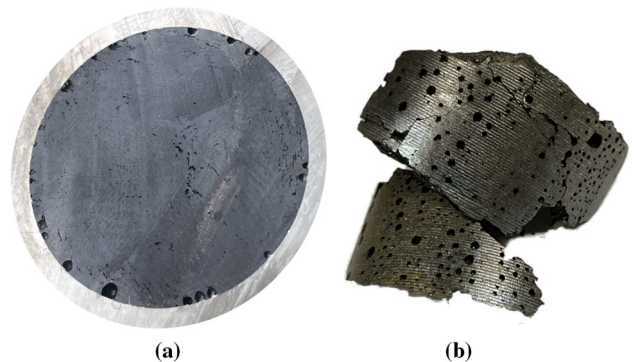


Fig. 5—(a) Cross-section of the solidified material in the Ni crucible; (b) Solidified material removed from the Ni crucible where traces of bubbles were observed.

C. SEM-EDS Analysis

The post-experimental analysis of the crucible and reference material interaction included SEM-EDS, showing that all crucibles interacted with the reference material. SEM images of the Fe, Ni, and Mo crucibles and the interactions with the reference material are presented in Figures 6(a)–(f). The images of the Fe crucible show that the crucible had softened and partly melted into the reference material in the form of distinct phases. The phase marked with “Fe” in Figures 6(a) and (b) originated from the Fe crucible, and the EDS analysis showed it was metallic iron. Fe was also found as FeS, as shown by the phase marked 3 in Figure 6(a). The sulfur content in the reference material came from the chemicals used in the synthesis.

Metallic Fe was mainly found at the interface towards the crucible, indicating that the Fe content gradually increased when moving from the center toward the interface. The chemical analysis was based on the solidified melt scraped off the crucible, meaning the more Fe-rich material at the interface was not included. The gradual change in the Fe content could affect the viscosity measurements as the material was not homogeneous. The results highlight the importance of post-experimental examinations after viscosity measurements, as the interaction varies between the *c/s* materials.

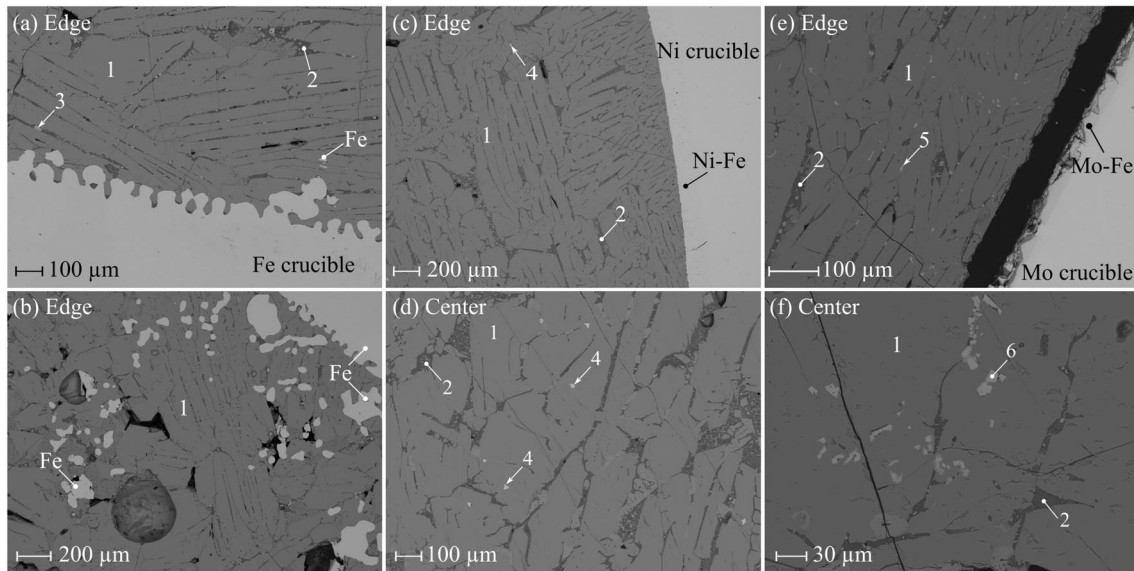


Fig. 6—SEM images of the (a) and (b) Fe; (c) and (d) Ni; and (e) and (f) Mo crucibles and the reference material interaction. The phase marked 1 is an Fe–Si–O phase, 2 is an Fe–Si–Al–O phase, 3 is an Fe–S phase, 4 is a Ni–Fe alloy, and the phases marked 5 and 6 are Mo-containing phases.

The crucibles holding the melt were slowly cooled in the furnace after the viscosity measurements, an Fe–Si–O phase (marked 1 in Figure 6) crystallized first, and then the remaining melt containing more Al_2O_3 solidified (number 2 in Figure 6). This was supported by thermodynamic calculations performed using FS, where Fe_2SiO_4 (olivine phase) was the first phase to crystallize. The phases marked 1 and 2 were found in all post-experimental materials regardless of the crucible used.

SEM images of the post-experimental Ni crucible, the material/crucible interaction, and from the center are presented in Figures 6(c) and (d), respectively. Ni was found to be a distinct phase in the reference material, which contained approximately 85 wt pct Ni and 15 wt pct Fe. Ni was intermittently found in the oxide phase from 0.20 to 0.71 wt pct.

The Mo crucible interaction with the reference material and the crucible center are presented in Figures 6(e) and (f), respectively. The post-experimental material detached from the crucible creating a gap (black area, Figure 6(e)). Mo was found as bright phases (labeled 5) close to the crucible wall, indicating that the Mo crucible had partially dissolved into the reference material, supported by the chemical analysis. The bright Mo phases also contained Fe, Al, and approximately 1 wt pct Si. In the reference material at the center of the crucible, Mo was found to be in a phase mainly containing Fe (40.8 wt pct), Mo (37.1 wt pct), and O (21.0 wt pct), and small amounts of Al (1.0 wt pct) (6 in Figure 6(f)). The atomic content of the Mo-phase corresponded to a $\text{Mo}(\text{Fe}, \text{Al})_2\text{O}_4$ spinel. The mineralogy of the phase has not been confirmed with any additional method and was not shown in the equilibrium calculations using FS, as Mo was not included in the FToxid database. Westland and Webster^[31] studied the Mo distribution between slag and copper matte and metal and found Mo in Fe–Mo oxides in the slag phase.

The apparent composition of the oxides varied, with Mo contents from 15.5 to 53.3 pct.^[31] From the crystallization pattern, the Mo-phase could be a possible solid in the melt, where the Fe_2SiO_4 phase started to crystallize, pushing the Mo-phase and the remaining melt toward each other, and the remaining melt then crystallized as the darker, more Al-rich phase (labeled 2) with the already solid Mo-phase in it (labeled 6).

EDS point analyses from the post-experimental material using Fe, Ni, and Mo as *c/s* materials are presented in Figures 7(a)–(c), respectively. Fe was visually observed as metallic, approximately 0.1 mm into the reference material but varied as larger pieces occasionally detached from the crucible and moved further into the reference material, as observed in Figure 6(b). The distinct phases of Fe have a higher density than the reference material, meaning they settled through the melt. From the EDS point analyses presented in Figure 7(a), a clear edge was visible when moving from the crucible to the oxide phase. The solidified material was stable in composition, mainly containing an Fe–Si–O and Fe–Si–Al–O phase.

Figure 7(b) shows the EDS point analysis of the Ni crucible and the interaction with the reference material. A Ni–Fe alloy was observed in the crucible wall toward the post-experimental material (marked 4 in Figures 6(c) and (d)). Fe diffused approximately 0.2 mm into the crucible wall forming the Ni–Fe alloy. The Fe content decreased when the points moved into the Ni crucible, from approximately 25 wt pct Fe at the crucible edge to 100 wt pct Ni about 0.2 mm into the crucible. The diffusion of Fe into the Ni crucible will change the melt composition, affecting the viscosity measurements.

The formation of a gaseous phase was indicated when the solidified melt was removed from the crucibles, and traces of bubbles were observed (Figure 5). The chemical analysis confirmed the increased content of Fe_2O_3 using

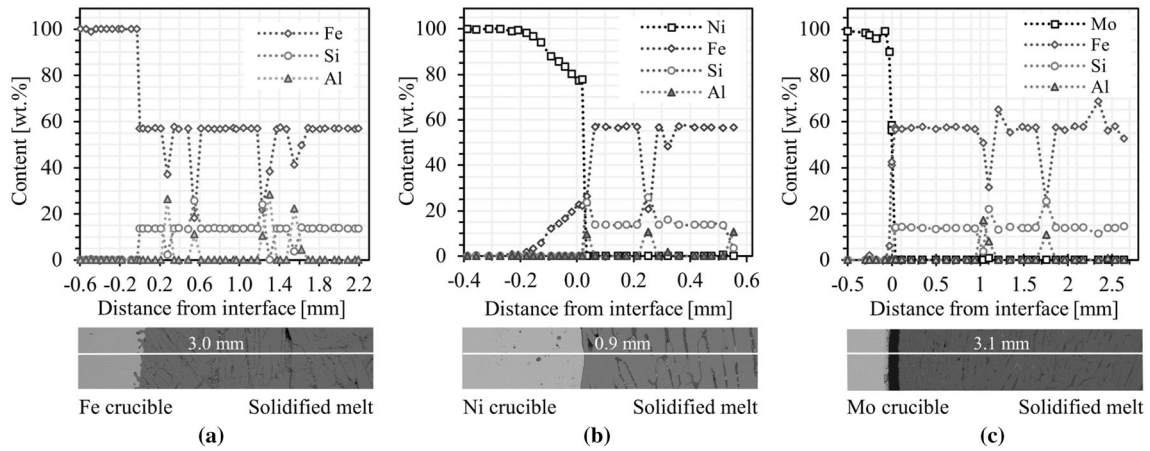


Fig. 7—EDS point analysis of the crucible interaction with the reference material for the (a) Fe, (b) Ni, and (c) Mo crucible.

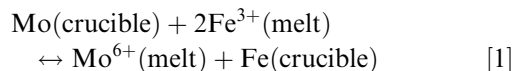
the Ni *c/s* material (Table I). The formed Ni–Fe alloy explained why the Fe_{tot} content was lower in the post-experimental material using the Ni *c/s* material.

Figure 7(c) shows the EDS point analysis of the Mo crucible and the interaction with the reference material. A Mo–Fe phase was observed at the crucible edge toward the post-experimental material (labeled Mo–Fe in Figure 6(e)), and Fe diffused approximately 0.08 mm into the crucible wall. The Mo–Fe phase contained at most 44 wt pct Fe (56 wt pct Mo) at the interface towards the solidified melt. The atomic percentage of Mo in the Mo–Fe phase varied between 42 and 55 at. pct, lowest close to the interface. Mo was not detected in the oxide phases containing Fe–Si–O and Fe–Si–Al–O. The diffusion of Fe into the Ni crucible was more extensive than into the Mo crucible, indicating that the interaction with the melt was stronger using the Ni crucible.

D. Mechanisms of Melt and Crucible Interactions

Mechanisms for the melt–crucible interaction are proposed based on chemical analyses, visual observations, and SEM–EDS analysis. In summary, Mo was found as a Mo–Fe phase in the crucible, as distinct Mo–Fe–O phases in the slag, and potentially as evaporated and condensed MoO_3 on the crucible wall. Possible reaction scenarios are shown in Figures 8(a)–(c). The valence states of Fe represent the melt composition as they were assumed to cause the interaction with the crucibles.

The interaction mechanism between the Mo crucible and Fe in the melt is suggested to start with the oxidation of Mo by Fe^{3+} or Fe^{2+} in the melt resulting in Fe and Mo^{6+} , shown in Figure 8(b) and Eq. [1].



Oxidized Mo forms distinct phases in the melt, as shown in Figures 6(e) and (f). The reduced Fe on the crucible–melt interface (Figure 8(b)) diffuses into the Mo crucible forming an intermetallic Mo–Fe phase (Figure 8(c)). The formation of the Mo–Fe phase in the

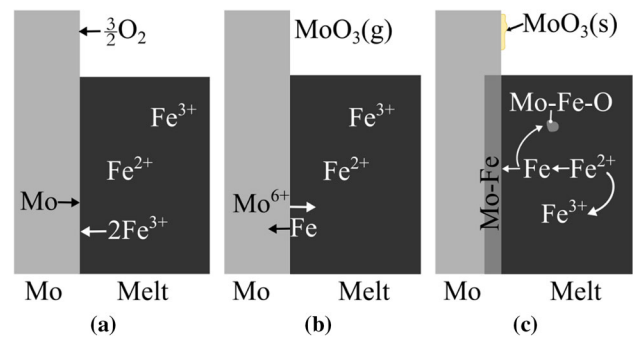
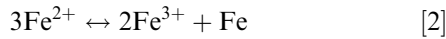


Fig. 8—Mechanisms for Mo interaction with the FeO – Fe_2O_3 – SiO_2 – Al_2O_3 melt (a) Mo was oxidized while reducing Fe^{2+}/Fe^{3+} in the melt, (b) Mo^{6+} (MoO_3) diffused into the melt while Fe diffused into the crucible forming the intermetallic Mo–Fe phase shown in (c) together with the identified Mo–Fe–O phase in the melt.

crucible decreases the activity of the Fe, pushing reaction [1] to the right. However, the formation of the Mo–Fe phase becomes a diffusion barrier in the crucible, limiting Fe from diffusing more than 0.08 mm into the crucible wall, as seen in Figure 6(c). The diffusion barrier can be explained with the Fe–Mo phase diagram shown in Figure 9. The identified Mo–Fe phase, ~42 at. pct Mo at the crucible interface is within the composition range of the μ -phase, which has been suggested to contain between 39 and 44 at. pct Mo.^[32] Fe appears limited to diffuse into the crucible when this phase is formed. At the interface between the intermetallic Mo–Fe phase and pure Mo, the composition corresponds to the σ -phase, suggested to contain between 42.9 and 56.7 at. pct Mo.^[32] The Mo–Fe phase in the crucible explains why the total iron content in the melt decreased using the Mo system.

Besides Mo oxidation, the intermetallic phase in the crucible can be formed by the reaction shown in Eq. [2]. When Fe in the melt diffuses into the crucible, the activity of Fe in the melt decreases, and reaction [2] is pushed to the right forming Fe^{3+} , thus increasing this content and decreasing the content of Fe^{2+} and Fe in the slag phase.



When Fe is used as a crucible, the activity of Fe in the crucible is unity pushing reaction [2] to the left, thus reducing Fe^{3+} to Fe^{2+} , which was confirmed in the chemical analysis. The sample from the Fe crucible had the lowest Fe^{3+} content and the highest Fe content, indicating that $\text{Fe}^{2+}/\text{Fe}^{3+}$ in the melt had been reduced during the viscosity measurements. This aligns with the theory that an Fe crucible will act as a buffer in the system, which will move towards the Fe–FeO conditions.^[15]

The Ni and melt interaction mechanisms are shown in Figures 10(a) and (b). Figure 10(a) shows the initial conditions where Ni in the crucible diffuses into the melt while $\text{Fe}^{2+}/\text{Fe}^{3+}$ was reduced into Fe. Fe diffused into the crucible forming the Ni–Fe alloy shown in Fig-

ure 10(b). The diffusion of Fe into the crucible forming the alloy decreases the Fe activity in the melt, pushing reaction [2] to the right, illustrated in Figure 10(b). Ni and Fe form a solid solution over the entire composition region at the experimental temperatures.^[33] The continuous solid solution drives smooth diffusion of the Fe atom into the Ni crucible. The diffusion was thus more extensive using the Ni crucible than the other crucibles, affecting the melt composition and $\text{Fe}^{2+}/\text{Fe}^{3+}$ ratio more extensively and thus the viscosity measurements.

Ni was also found in the oxide phase during the SEM–EDS analysis, implying that Ni partially dissolved into the melt, shown in Figure 10(a). The dissolved Ni could then react with Fe in the melt forming the Ni–Fe phase identified in Figures 6(c) and (d) and illustrated in Figure 10(b).

E. Viscosity During Homogenization

When the viscosity measurements started, the temperature was raised to 1723 K using Mo crucibles and 1623 K using Fe and Ni crucibles. The temperature was then allowed to become uniform in the furnace, crucible, reference material, and spindle for 60 minutes at a constant shear rate of 1 s^{-1} ; after that, the temperature was held constant for 30 minutes with a constant shear rate of 4 s^{-1} . During these 30 minutes, the melt became homogeneous in composition and temperature, which meant that the viscosity should decrease theoretically as the temperature increased in this stage.

The viscosity measurements during the first homogenization time are shown in Figure 11. The readings with the Mo spindle were stable throughout the whole time, whereas the viscosity measured with the Fe spindle was unstable, and the viscosity increased. The change in viscosity indicates that the Fe *c/s* material interacted with the melt. The increased viscosity of the melt was explained by the distinct phases of Fe, which dissolved into the reference material, causing structural changes in

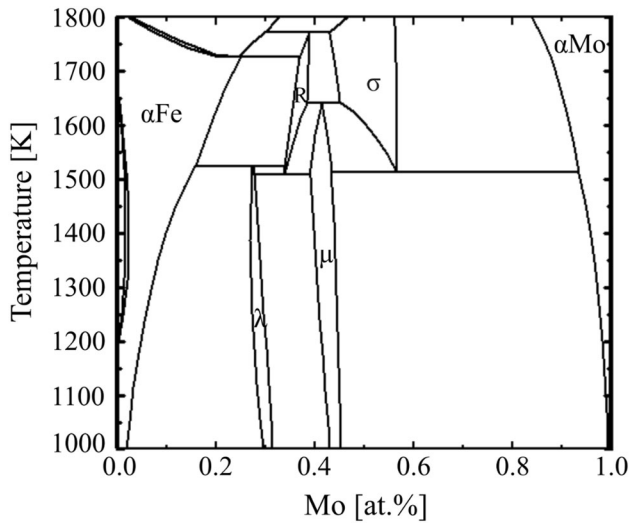


Fig. 9—Fe–Mo phase diagram. Calculated using the phase diagram module of FactSage 8.2^[30] with the FSstel database.

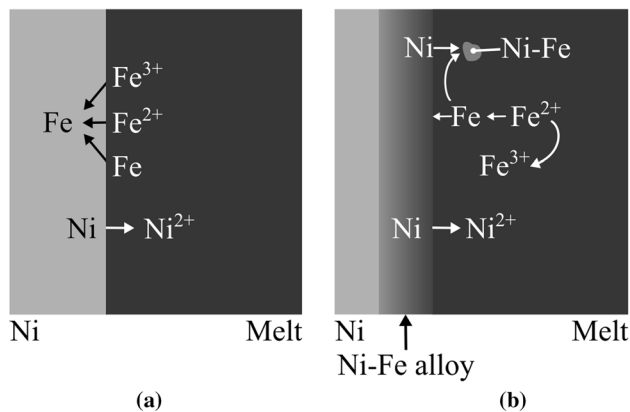


Fig. 10—Mechanisms for Ni interaction with the $\text{FeO–Fe}_2\text{O}_3\text{–SiO}_2\text{–Al}_2\text{O}_3$ melt, (a) shows the initial condition where Ni is oxidized, forming Ni^{2+} , which diffuses into the melt, while $\text{Fe}^{2+}/\text{Fe}^{3+}$ is reduced and diffuses into the crucible forming the Ni–Fe alloy shown in (b) together with the Ni–Fe phase identified in the melt.

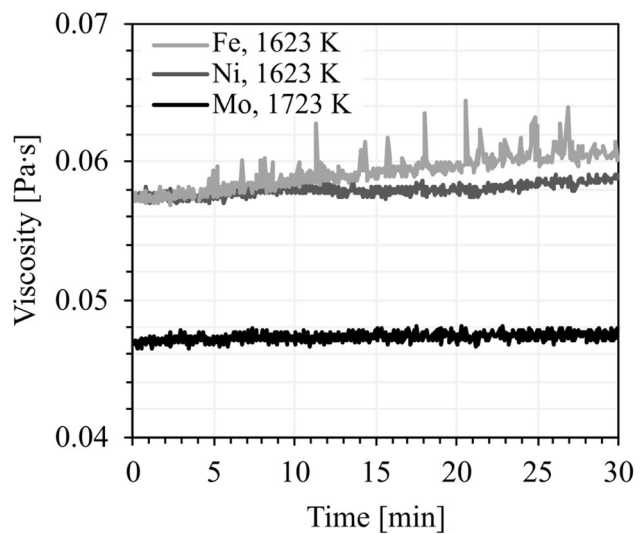


Fig. 11—Viscosity measurements during homogenization at the first experimental temperature using Mo, Fe, and Ni as the *c/s* material.

the oxide system. The melt and crucible/spindle interactions and the changed geometries also contributed to the unstable reading. Inconsistent measurements of pre-homogenized melts can be because of reactions between the sample and the atmosphere, interaction with the c/s material, or poor temperature control.^[34] During the viscosity measurements, the furnace atmosphere and the temperature control were the same in all experiments, which excludes these parameters as a possible contribution to the unstable measurements. The inconsistent readings were thus due to the interaction between the melt and the c/s material.

The viscosity during the homogenization time using the Ni c/s material was more stable than when using Fe. However, an increase in viscosity was observed, indicating an interaction with the Ni c/s . The disagreement in viscosity between the measurements made by Ni/Fe and the Mo c/s was explained by the temperature difference (100 K) at the first homogenization time.

F. Viscosity Measurements

The average viscosities and the sample standard deviation of the synthetic $\text{FeO}_x\text{-SiO}_2\text{-Al}_2\text{O}_3$ melt measured with the different c/s materials are presented in Figure 12, together with the calculated viscosity. Overall, the viscosity decreased with increasing temperature. The viscosity was measured using different shear rates (1, 2, 4, 8, and 16 s^{-1}), the sample standard deviation for the replicates overlapped, and the statistical analysis showed no significant difference in the measured viscosity concerning the shear rate. This means that the melt, regardless of c/s materials used, behaved as Newtonian fluids. The torque readings were most stable when the shear rate was 16 s^{-1} , and the data presented in Figure 12 were obtained using this shear rate.

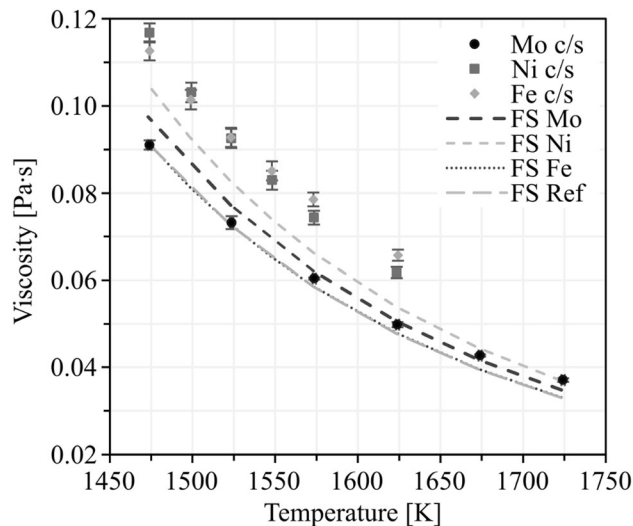


Fig. 12—Viscosity measurements with Fe, Mo, and Ni as the c/s material and the calculated viscosity using FS for the reference material (FS Ref) and the post-experimental compositions.

The most significant sample standard deviation between the three replicates using Mo as c/s material was 0.002 Pa s (1524 K), corresponding to 2.0 pct of the measured viscosity. The sample standard deviations indicated that the rheometer had good reproducibility. The most significant sample standard deviations for the Ni and Fe c/s materials were 0.002 and 0.003 Pa s , respectively (1499 K). Average $\text{FeO}_x\text{-SiO}_2\text{-Al}_2\text{O}_3$ melt viscosities using the c/s materials at various temperatures are shown in Table II.

The statistical analysis of the data showed that the viscosity measurements of the reference material performed using Mo as c/s material significantly differed from those when Fe and Ni were used at all temperatures investigated. The viscosity using the Mo c/s material was between 23 and 32 pct lower than when Fe and Ni were used, as shown in Figure 12. When the viscosity data using the Fe and Ni c/s were statistically analyzed, the viscosity measurements at the two highest temperatures (1624 K and 1573 K) significantly differed with a significance level of 0.05. The statistical analysis indicated that the viscosity of the reference material using Fe and Ni as c/s material differed at the beginning of the measurement but not at the end. According to the curvature of the viscosity-temperature line in Figure 12, the viscosity using Ni as c/s material had a steeper slope than the other two. However, in general, the viscosity measurements of the $\text{FeO}_x\text{-SiO}_2\text{-Al}_2\text{O}_3$ melt using Fe and Ni as c/s materials were in good agreement, consistent with the study by Viswanathan *et al.*^[3] where viscosity measurements were performed using Fe and Ni as c/s materials.

The calculated viscosity of the post-experimental composition using Fe as the c/s material was almost identical to the calculated viscosity of the reference material composition, implying that the Fe c/s affected the composition the least. However, this does not agree with the measured viscosity using the Fe c/s due to the melt interaction and changed geometries. The calculated viscosity when Mo was used as the c/s material differed between 1.6 and 7.0 pct from the measured viscosity; the difference was highest at the lowest temperature. The partial dissolution of Mo was assumed to increase over time if equilibrium between the c/s material and the reference material was not reached. Mo is not included in the database used for the viscosity calculations, which explains why the calculated viscosity diverged the most from the experimental values at the last measuring point, assuming that the Mo content was highest at the end. Additionally, the measured viscosity using the Mo c/s had a minor difference from the calculated viscosity of the reference material.

The viscosities measured using Fe and Ni as the c/s material differed from the calculated viscosity values, and the deviation was, at the most, 13 pct using Ni and 27 pct higher using Fe as the c/s material. One explanation for the difference was the melt and c/s interactions and the stability of the spindle during the measurements. The interaction between the Fe c/s material changed the composition of the reference material and the crucible and spindle geometries, increasing the viscosity shown during the

Table II. The Average Viscosity Obtained Using Mo, Ni, or Fe as the *c/s* Material at Different Temperatures, the Calculated Viscosity (FS), and the Activation Energy

<i>c/s</i> Material	Temperature (K)	Viscosity (Pa s)	Calculated Viscosity, FS (Pa s)	Activation Energy, E_a (kJ/mol)	Material Constant, (10^{-4} Pa s)
Mo	1724	0.037	0.035	76.5	1.79
	1674	0.043	0.042		
	1624	0.050	0.051		
	1574	0.060	0.062		
	1524	0.073	0.077		
	1474	0.091	0.098		
Ni	1724	—	0.037	85.2	1.16
	1674	—	0.044		
	1624	0.062	0.054		
	1573	0.074	0.066		
	1548	0.083	0.074		
	1523	0.093	0.083		
	1499	0.103	0.093		
	1474	0.117	0.105		
Fe	1724	—	0.033	70.8	3.55
	1674	—	0.034		
	1624	0.066	0.048		
	1573	0.079	0.059		
	1548	0.085	0.065		
	1523	0.093	0.073		
	1499	0.101	0.081		
	1474	0.113	0.092		

homogenization time. The post-experimental material using Fe as a *c/s* material contained 1.07 wt pct Fe_{met} and large pieces of Fe ($> 200 \mu m$) were observed. Distinct phases in the melt could similarly affect the viscosity as if solids were present. A well-known model based on Einstein's approach was developed by Roscoe,^[35] known as the Einstein–Roscoe equation, shown in Eq. [3], where the viscosity increases when the melt contains solid particles.

$$\eta = \eta_0(1 - af)^{-n} \quad [3]$$

where η is the viscosity of a melt containing solids, η_0 is the viscosity of a melt without solids, f is the volume fraction of solid particles, and a and n are constants. Wright et al.^[36] studied the viscosity of a CaO–MgO–Al₂O₃–SiO₂ slag with the addition of spinel particles at 1646 K. The dependence of the viscosity on the amount of solid addition could be described by the Einstein–Roscoe equation. Zhen et al.^[37] studied the viscosity of CaO–MgO–Al₂O₃–SiO₂–TiO₂ melts containing TiC particles and showed that the viscosity increased gradually when TiC particles were added. Possible solid or distinct phases originating from the *c/s* material in the oxide system studied can thus increase the viscosity. However, the volume fraction of the Fe particles was not confirmed, and thus the effect on the viscosity. The Fe particles were most frequently found near the interface between the melt and the crucible, and the effect on the viscosity could instead have been caused by the solid phases on the spindle and at the liquid level.

G. Activation Energy

The viscosity of liquids is well known to decrease with increasing temperature.^[5,38,39] The temperature dependence of the viscosity for a given melt composition can be described by an Arrhenius-type relationship^[40], as shown in Eq. [4].

$$\eta = A \exp\left(\frac{E_a}{RT}\right) \quad [4]$$

where η is the viscosity (Pa s), A is the pre-exponential factor (Pa s), E_a is the activation energy of flow (J/mol), T is the absolute temperature (K), and R is the gas constant (8.341 J/mol K). The activation energy of flow provides a reference for the variation in internal friction of viscous flow and reflects the changes in slag structure over a temperature interval.^[41] The activation energy for the average viscosity using the different *c/s* materials was calculated according to Eq. [5].

$$\ln \eta = \ln A + \frac{E_a}{R} \left(\frac{1}{T}\right) \quad [5]$$

The natural logarithm of the average viscosity for each *c/s* material was plotted against $1000/T$ and is shown in Figure 13. The plot reveals that all data obtained from each *c/s* material have a linear fit with an R^2 value above 99.9 pct, which indicates that the viscosity of the reference material using the three different *c/s* materials in this study followed Arrhenius behavior. The average activation energy' of the three

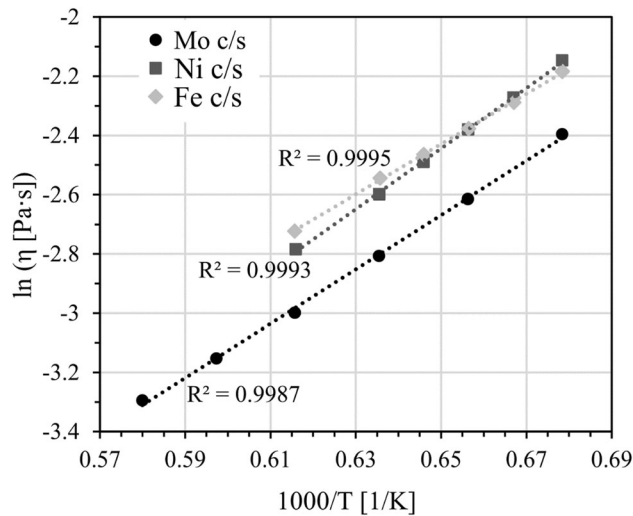


Fig. 13—Natural logarithm of the viscosity vs $1000/T$, trendline, and R^2 values.

replicates using the c/s materials is presented in Table II. The activation energy of the $\text{FeO}_x\text{-SiO}_2\text{-Al}_2\text{O}_3$ melt using the c/s materials is presented in descending order for Ni, Mo, and Fe, with activation energies of 85.2, 76.5, and 70.8 kJ/mol, respectively. The statistical analysis showed that when using Ni as the c/s material, the activation energy significantly differed from when using Fe and Mo as the c/s materials. The activation energy has previously been linked to the strengths of bonds that need to be broken to accomplish flow.^[42] The activation energy in the Arrhenius-type relationship explains the curvature of the viscosity line plotted against the temperature (Figure 12), which meant that melts with higher activation energy were more strongly affected by temperature changes.

The lower activation energy of the oxide system using Fe as c/s material is explained by the higher content of Fe. If the dissolutions happened over time, it theoretically meant that the Fe content was lowest at the beginning of the measurements and then increased gradually with time. In the literature, there are clear descriptions of where the viscosity decreased with increasing Fe/SiO₂ content in the melt.^[2,5,26,27] The effect was more pronounced at lower temperatures and lower Fe/SiO₂ ratios.^[26] The effect of the Fe/SiO₂ ratio on the viscous behavior was explained by structural changes in slag, where a higher SiO₂ content meant a more complex network structure. If the FeO content increased and the Fe₂O₃ content decreased gradually and thus decreased the viscosity during the measurements, the curvature of the viscosity line became less pronounced, and hence, the activation energy decreased. FeO is known to be a basic oxide that breaks $[\text{SiO}_4]^{4-}$ network structure in oxide systems and thus reduces the viscosity.^[2] The viscosity of the reference material using Fe as the c/s material was higher than the viscosity measured with Ni as the c/s material at the first measurement and lower at the last measurement.

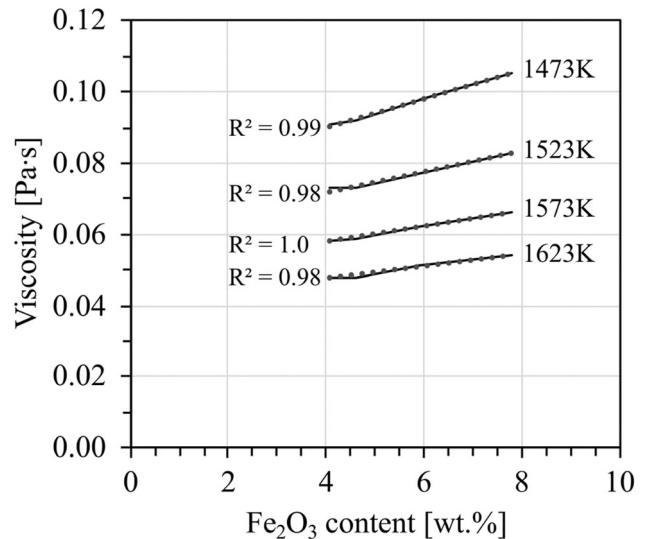


Fig. 14—Calculated viscosities (FS) at different temperatures vs the Fe_2O_3 content in the post-experimental material, the trendlines (dotted), and R^2 values.

The post-experimental analysis of the reference material using Ni as the c/s material had the highest content of Fe_2O_3 . From the visual observations and the SEM-EDS analysis, a Ni-Fe alloy was observed in the Ni crucible, and traces of gas bubbles were observed near the interface to the Ni crucible, indicating the interaction between the melt and crucible. The system lost oxygen when Fe diffused into the Ni crucible and oxidized FeO into Fe_2O_3 . If the content of Fe_2O_3 increased over time, it explains why the curvature (Figure 12) and hence the activation energy was most pronounced for the measurements using Ni as the c/s material. Viswanathan *et al.*^[3] found a sharp viscosity increase when the Fe_2O_3 content reached approximately 7 wt pct in an FeO-SiO_2 slag using a Ni c/s material. The Fe/SiO₂ ratio in the post-experimental material was approximately 1.8, which meant that the amphoteric compound Fe_2O_3 acted as an acidic oxide in the melt and thus formed a network with $[\text{SiO}_4]^{4-}$, which meant an increased viscosity, more ordered structure, and therefore higher activation energy.

The viscosity calculation using FS indicated that the post-experimental material using the Ni c/s had the highest viscosity at lower temperatures. Additionally, it showed that the viscosity was correlated with the Fe_2O_3 content at a specific temperature, as shown in Figure 14, where the calculated viscosity at different temperatures is plotted against the Fe_2O_3 content. The Fe_2O_3 content in the post-experimental material plotted against the respective activation energies resulted in a linear relationship with a R^2 value of 99.99 pct, strengthening that the crucible affected the Fe_2O_3 content in the melt and, thus, the structure and activation energy.

The calculated pre-exponential factor, A , is presented in Table II, and it was greatest when Fe was used as the c/s material and smallest when Ni was used as the c/s material. When Fe was used as the c/s material, the

pre-exponential factor differed significantly, with a significance level of 0.05, from when using the other two *c/s* materials. The pre-exponential factor was dependent upon the molten material structure. The variation in this factor obtained by measuring the viscosity of the same reference material but with different *c/s* materials indicated that the different *c/s* materials change the melt structure, where the Fe *c/s* material increased the pre-exponential factor and thus the viscosity.

Additionally, during the viscosity measurements, the Fe spindle and crucible geometries were changed by solid precipitation on the spindle and at the liquid level. The Fe spindle could thus not be used for more than one viscosity measurement experiment, and the affected spindle caused instability in the viscosity measurements. The Fe *c/s* material is thus not a preferable crucible choice for high-temperature viscosity measurements.

IV. CONCLUSIONS

One important factor concerning rheological studies is the interaction between the melt and the *c/s* material. Post-experimental chemical analyses are often performed and reported, but not how the interaction influences the viscosity measurements. For more reliable viscosity measurements in the FeO–SiO₂-based system, viscosity measurements were performed using three different *c/s* materials, Mo, Fe, and Ni, to examine the interaction between the *c/s* material and the melt and the effect on the viscosity. The study aimed to determine which *c/s* material had the most negligible interaction with the melt, with minimum viscosity impact and the highest reproducibility.

The results of the present study indicated that interactions between crucibles and melts always occur. However, choosing an appropriate *c/s* material limits the interactions with the melt and the influence on the viscosity. In this study, when the post-experimental analysis and the viscosity measurements were considered, Mo influenced the viscosity measurements the least and gave the most stable viscosity data with the best reproducibility at different temperatures. The Mo *c/s* allows the most comprehensive temperature range during the viscosity measurements among the evaluated materials. Thus, Mo was the preferred *c/s* material for the FeO–SiO₂–Al₂O₃ system, which can be expanded into an industrially relevant system based on FeO–SiO₂.

ACKNOWLEDGMENTS

The project was conducted within the Center for Advanced Mining and Metallurgy (CAMM) at Luleå University of Technology and financially supported by Boliden AB through Bolidenpaketet.

FUNDING

Open access funding provided by Lulea University of Technology.

CONFLICT OF INTEREST

The authors declare that they have no conflict of interest.

OPEN ACCESS

This article is licensed under a Creative Commons Attribution 4.0 International License, which permits use, sharing, adaptation, distribution and reproduction in any medium or format, as long as you give appropriate credit to the original author(s) and the source, provide a link to the Creative Commons licence, and indicate if changes were made. The images or other third party material in this article are included in the article's Creative Commons licence, unless indicated otherwise in a credit line to the material. If material is not included in the article's Creative Commons licence and your intended use is not permitted by statutory regulation or exceeds the permitted use, you will need to obtain permission directly from the copyright holder. To view a copy of this licence, visit <http://creativecommons.org/licenses/by/4.0/>.

REFERENCES

1. R.H. Eric: *J. S. Afr. Inst. Min. Metall.*, 2004, vol. 104, pp. 499–510.
2. M. Kucharski, N.M. Stubina, and J.M. Toguri: *Can. Metall. Q.*, 1989, vol. 28, pp. 7–11.
3. N.N. Viswanathan, F.Z. Ji, D. Sichen, and S. Seetharaman: *ISIJ Int.*, 2001, vol. 41, pp. 722–27.
4. S. Nagraj, M. Chintinne, M. Guo, and B. Blanpain: *JOM*, 2022, vol. 74, pp. 274–82.
5. M. Chen, S. Raghunath, and B. Zhao: *Metall. Mater. Trans. B*, 2013, vol. 44B, pp. 506–15.
6. S. Wright and L. Zhang: in *VII Int. Conf. on Molten Slags Fluxes and Salts*, South African Institute of Mining and Metallurgy, Cape Town, South Africa, 2004, pp. 231–36.
7. K.C. Mills, L. Chapman, A.B. Fox, and S. Sridhar: *Scand. J. Metall.*, 2001, vol. 30, pp. 396–403.
8. M.E. Schlesinger, M.J. King, K.C. Sole, and W.G. Davenport: *Extractive Metallurgy of Copper*, 5th ed. Elsevier Ltd, Oxford, 2011.
9. P.J. Mackey: *Can. Metall. Q.*, 1982, vol. 21, pp. 221–60.
10. S. Mostaghel, C. Samuelsson, and B. Björkman: *Int. J. Min. Metall.*, 2013, vol. 20, pp. 234–45.
11. T.A. Utigard: *Scand. J. Metall.*, 1994, vol. 23, pp. 37–41.
12. H. Shen and E. Forssberg: *Waste Manag.*, 2003, vol. 23, pp. 933–49.
13. R. Reddy and Z. Zhang: *Recycling of Metals and Engineered Materials*, TMS, Pittsburgh, 2000, pp. 153–63.
14. B. Wang, H. Yang, Z. Jin, Z. Liu, and M. Zou: *Metals*, 2022, vol. 12, pp. 1–18.
15. B. Mysen and P. Richet: *Silicate Glasses and Melts*, 2nd ed. Elsevier, Amsterdam, 2018.
16. W.D. Callister and D.G. Rethwisch: *Materials Science and Engineering*, 9th ed. Wiley, New York, 2014.

17. A.Y. Ilyushechkin, M.A. Duchesne, S.S. Hla, A. MacChi, and E.J. Anthony: *J. Mater. Sci.*, 2013, vol. 48, pp. 1053–66.
18. M. Allibert, H. Gaye, J. Geiseler, D. Janke, B.J. Keene, D. Kirner, M. Kowalski, J. Lehmann, K. Mills, D. Neuschütz, R. Parra, C. Saint-Jours, P. Spencer, M. Susa, M. Tmar, and E. Woermann: *Slag Atlas*, 2nd ed. Verlag Stahleisen, Düsseldorf, 1995.
19. Y. Shen, J. Chong, Z. Huang, J. Tian, W. Zhang, X. Tang, W. Ding, and X. Du: *Materials*, 2019, vol. 12, pp. 1–16.
20. K. OuYang, Z.H. Dou, T.A. Zhang, and Y. Liu: *J. Min. Metall. B*, 2020, vol. 56, pp. 27–33.
21. K.H. Sandhage and G.J. Yurek: *J. Am. Ceram. Soc.*, 1990, vol. 73, pp. 3633–42.
22. Y.J. Park, Y.M. Cho, W.Y. Cha, and Y.B. Kang: *J. Am. Ceram. Soc.*, 2020, vol. 103, pp. 2210–24.
23. O. Vergote, I. Bellemans, A. van den Bulck, and K. Verbeke: *Metall. Mater. Trans. B*, 2021, vol. 52B, pp. 3646–59.
24. S. Mostaghel, T. Matsushita, C. Samuelsson, B. Björkman, and S. Seetharaman: *Miner. Process. Extr. Metall.*, 2013, vol. 122, pp. 42–48.
25. H.-S. Park, S.S. Park, and I. Sohn: *Metall. Mater. Trans. B*, 2011, vol. 42B, pp. 692–99.
26. Z. Jin, B. Wang, Z. Liu, H. Yang, M. Zou, and Y. Fu: *Metall. Mater. Trans. B*, 2022, vol. 53B, pp. 9–15.
27. G.H. Kaiura, J.M. Toguri, and G. Marchant: *Can. Metall. Q.*, 1977, vol. 16, pp. 156–60.
28. M. Chen, S. Raghunath, and B. Zhao: *Metall. Mater. Trans. B*, 2013, vol. 44B, pp. 820–27.
29. F. Anton Paar GmbH: <https://www.anton-paar.com/corp-en/products/details/furnace-rheometer-systems-frs-1600-and-frs-1800/>, (accessed 11 March 2022).
30. C.W. Bale, E. Bélisle, P. Chartrand, S.A. Decterov, G. Eriksson, A.E. Gheribi, K. Hack, I.H. Jung, Y.B. Kang, J. Melançon, A.D. Pelton, S. Petersen, C. Robelin, J. Sangster, P. Spencer, and A.D. van Ende: *Calphad*, 2016, vol. 54, pp. 35–53.
31. A.D. Westland and A.H. Webster: *Can. Metall. Q.*, 1990, vol. 29, pp. 217–25.
32. A.F. Guillermet: *Bull. Alloy Phase Diagr.*, 1982, vol. 3, pp. 359–67.
33. G.I. Silman: *Met Sci Heat Treat.*, 2012, vol. 54, pp. 106–112.
34. M.A. Duchesne, A.Y. Ilyushechkin, R.W. Hughes, D.Y. Lu, D.J. McCalden, A. MacChi, and E.J. Anthony: *Fuel*, 2012, vol. 97, pp. 321–28.
35. R. Roscoe: *Br. J. Appl. Phys.*, 1952, vol. 306, pp. 267–69.
36. S. Wright, L. Zhang, S. Sun, and S. Jahanshahi: *Metall. Mater. Trans. B*, 2020, vol. 51B, pp. 97–104.
37. Y.L. Zhen, G.H. Zhang, and K.C. Chou: *Metall. Mater. Trans. B*, 2015, vol. 46B, pp. 155–61.
38. L. Deng, S. Wang, Z. Zhang, Z. Li, R. Jia, F. Yun, H. Li, Y. Ma, and W. Wang: *Mater. Chem. Phys.*, 2020, vol. 251, pp. 1–9.
39. F.-Z. Ji, D. Sichen, and S. Seetharaman: *Metall. Mater. Trans. B*, 1997, vol. 28B, pp. 827–34.
40. P. Atkins and J. de Paula: *Atkins Physical Chemistry*, 9th ed. Oxford University Press, Oxford, 2009.
41. G. Urbain, Y. Bottinga, and P. Richet: *Geochim. Cosmochim. Acta*, 1982, vol. 46, pp. 1061–72.
42. B. Mysen: *Eur. J. Miner.*, 2003, vol. 15, pp. 781–802.

Publisher's Note Springer Nature remains neutral with regard to jurisdictional claims in published maps and institutional affiliations.